Chapter 4 Monotonic Shear Wall Tests

4.1 Introduction

The five shear wall configurations described in Section 3.2 were monotonically tested, displacing the top of the shear wall six inches over a ten minute period. Monotonic loading was described in Section 3.6. Data from six LVDT's, measuring displacements of the wall during testing, and load cell were collected 10 times per second. Each of the five wall configurations was tested once. Of interest was data concerning ultimate load capacity and drift at capacity, elastic stiffness, ductility, movement of the end studs, and slip of the tie-down anchors relative to the tie-down stud.

4.2 Property Definitions

This section defines terms used to descibe and analyze the data determined for the monotonic shear wall tests.

4.2.1 Load-Displacement Curves

Figure 4.1 is a typical monotonic load-drift curve and illustrates terms defined in this section. From the load-drift curve, specimen capacity and its corresponding drift, elastic stiffness, and load resistance and drift at failure were determined. As defined in Section 3.5, drift is displacement of the top of the wall minus displacement of the bottom of the wall.

Capacity, F_{max}, was determined as the maximum load resisted by the wall. Δ_{max} was defined as the drift corresponding to capacity.

Elastic stiffness, k_e, was defined as the secant stiffness taken at 40% of capacity.

Load resistance at failure, $F_{failure}$, was determined as the highest load carried by the wall before a significant decrease in strength. Drift at failure, $\Delta_{failure}$, was defined as the corresponding drift.

4.2.2 Equivalent Elastic-Plastic Curve

An equivalent energy elastic-plastic curve, used for comparison purposes, was determined for each wall. This artificial curve, as shown in Figure 4.2, depicts how an ideal perfectly elastic - plastic wall would perform and dissipate an equivalent amount of energy as the actual specimen tested. The equivalent elastic-plastic curve (EEPC) was defined so that the area under the EEPC is equal to the area under the load-displacement curve from 0 in. drift to $\Delta_{failure}$. The elastic portion of the EEPC contains the origin and has a slope equal to the elastic stiffness, k_e. The plastic portion of the EEPC is a horizontal line positioned so that the EEPC and load-displacement curve areas are equal (i.e. areas A1 and A2 in

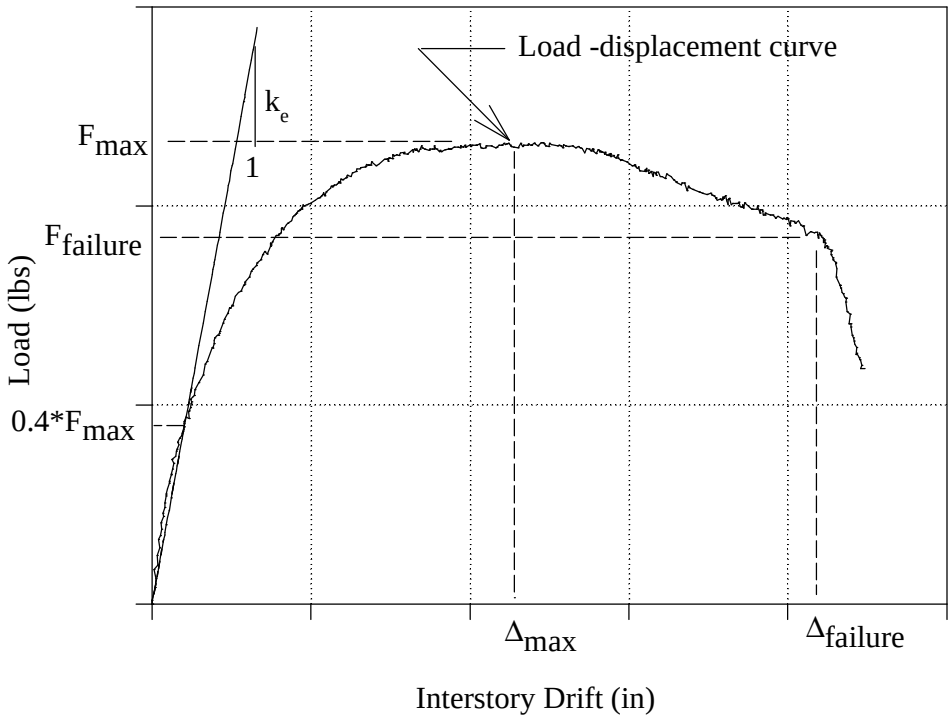

Figure 4. 1 - Typical load-drift curve for monotonic shear wall test

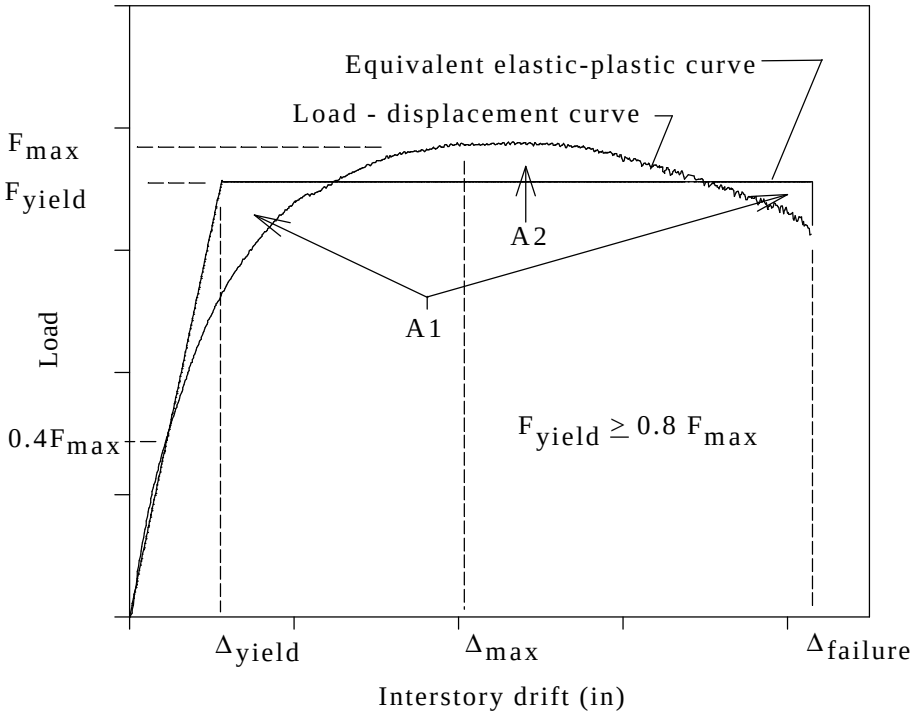

Figure 4. 2- Typical equivalent elastic-plastic curve

Figure 4.2 are equal). Displacement at yield, Δ_{yield}, and load at yield, F_{yield}, were defined as the intersection of the elastic and plastic lines of the EEPC. F_{yield} must be greater than or equal to 80% of F_{max}. This definition of the EEPC was also used in the cyclic tests, and is similar to that used in the sequential phased displacementtest developed by the Joint Technical Coordinating Committee on Masonry Research (TCCMAR) for the United States - Japan Coordinated Earthquake Research Program and defined by Porter (1987).

Ductility is determined from the EEPC and is defined as:

$$D = \frac{\Delta_{failure}}{\Delta_{yield}} \tag{4.1}$$

where D is ductility, $\Delta_{failure}$ is drift corresponding to failure, and Δ_{yield} is drift corresponding to yield.

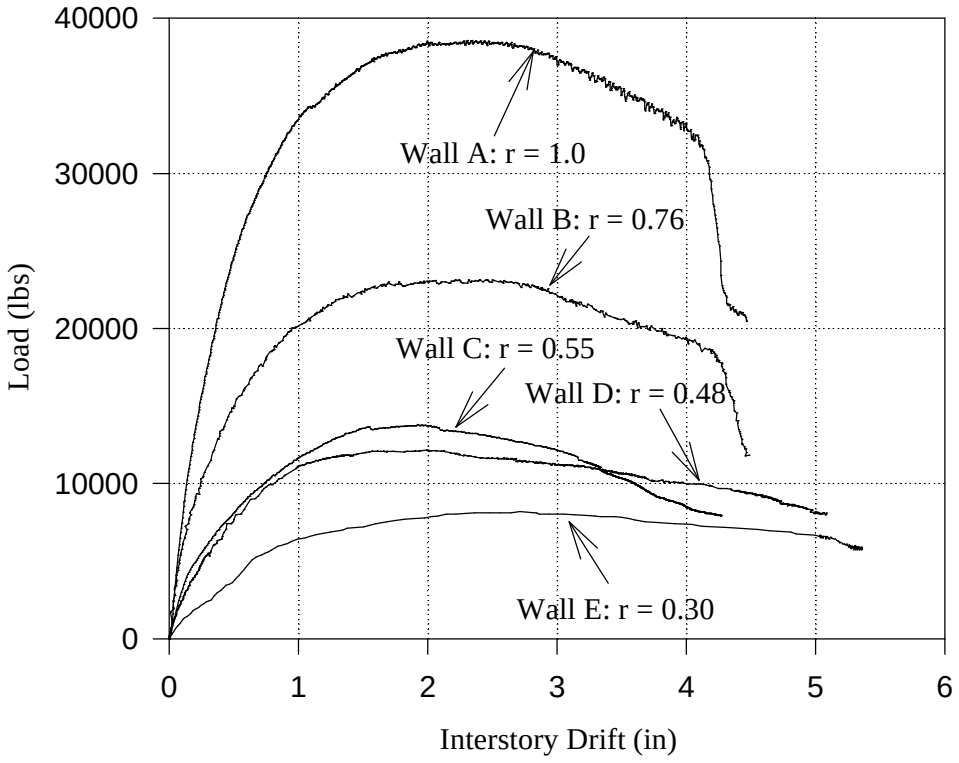

Figure 4. 3- Monotonic load-drift curves for the five shear wall configurations examined

4.3 Monotonic Test Results

This section presents the monotonic test results from the five shear wall configurations. Data concerning load resistance, drift, stiffness and ductility is examined.

4.3.1 Strength and deflection

Figure 4.3 plots load as a function of drift for the five wall configurations tested. As expected, elastic stiffness and capacity of each wall increased as the area of openings

decreased. As shown in Figure 4. 3, Wall A (r = 1.0) and Wall B (r = 0.76) experienced a sudden drop in load resistance during the test. Wall D (r = 0.48) and Wall E (r = 0.30) were able to continue resisting load past 5.0 in. (127 mm) drift. Wall C (r = 0.55) did not experience a sudden drop in load resistance, but lost its ability to resist load at a rate similar to Walls A and B.

As given in Table 4.1 and illustrated as a function of sheathing area ratio in Figure 4.4, capacity, F_{max}, ranged from 8.2 kips (36.5 kN) to 38.8 kips (172.6 kN). This represents a 79% change in capacity when the fully sheathed wall capacity is used as the basis for comparison. A best fit regression was performed with the data and plotted in Figure 4.4, resulting in the following third order equation for capacity as a function of sheathing area ratio:

$$F_{max} = 33.48 \cdot r - 37.06 \cdot r^2 + 42.48 \cdot r^3 \qquad (4.2)$$

where F_{max} is capacity and r is sheathing area ratio.

Table 4. 1: Monotonic data of five shear wall configurations examined

	Wall A	Wall B	Wall C	Wall D	Wall E
	r = 1.0	r = 0.76	r = 0.55	r = 0.48	r = 0.30
F_{max} (kips)	38.8	23.1	13.8	12.1	8.2
Δ_{max} (in)	2.0	2.2	1.9	1.6	2.7
F_{yield} (kips)	35.6	20.9	11.8	10.6	7.5
Δ_{yield} (in)	0.56	0.48	0.55	0.57	0.98
$F_{failure}$ (kips)	31.0	18.7	8.6	7.9	6.6
$\Delta_{failure}$ (in)	4.14	4.18	4.00	5.04	5.05
k_e (kips/in)	63.7	43.7	22.2	19.4	7.8
F_{yield}/F_{max}	0.92	0.90	0.86	0.88	0.91
Ductility	7.4	8.7	7.3	8.8	5.2

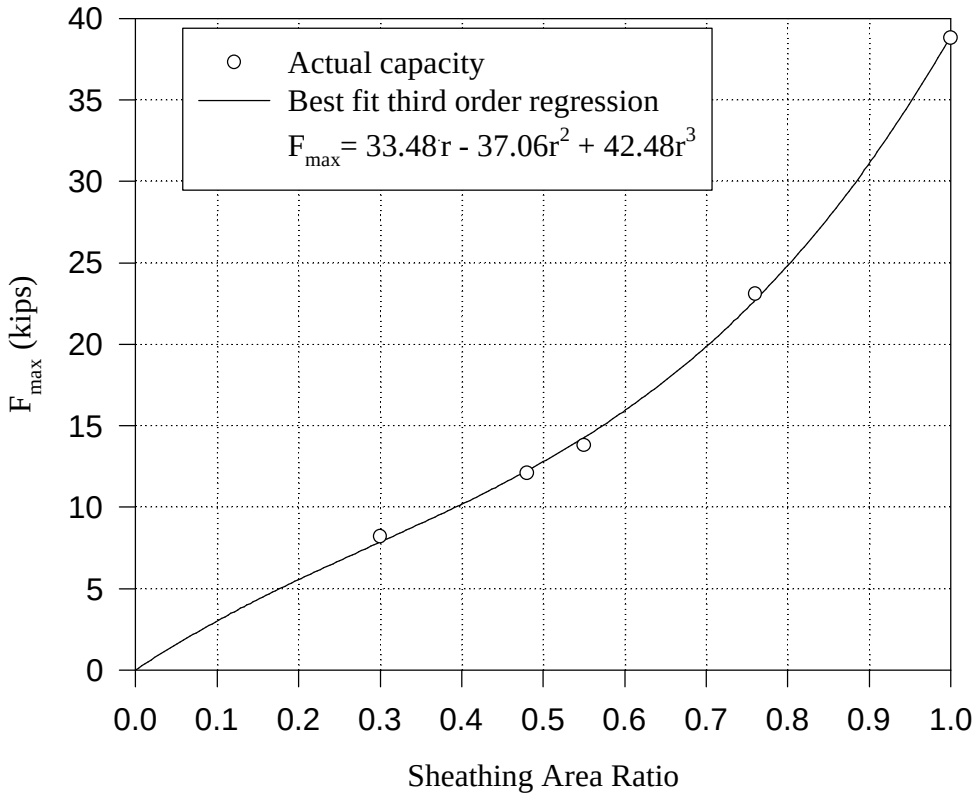

Figure 4. 4- Monotonic capacity of the five shear wall configurations examined plotted against sheathing area ratio

As shown in Figure 3.1, Walls C and D differ only by one sheathing panel below an opening. Wall C contains a 12 ft. (3.7 m) window, while Wall D contains a 12 ft. (3.7 m) garage door. Current design practices does not include sheathing above and below openings to resist shear in design. However, Table 4.1 shows that capacity of Wall C was 13.8 kips (61.4 kN) and the capacity of Wall D was 12.1 kips (53.8 kN). Clearly, the 2.5 ft. x 12 ft. (0.8 m x 3.7 m) sheathing panel below the 12 ft. (3.7 m) opening resists shear. It is also noted that failure of Wall C occurred at a lower drift than Wall D, resulting in a less ductile wall configuration.

As given in Table 4.1, displacement corresponding to capacity, $\Delta_{max,}$ ranged from 1.6 in. (41 mm) to 2.7 in. (69 mm), with Wall D (r = 0.48) having a Δ_{max} of 1.6 in. (41 mm) and Wall E (r = 0.30) having a Δ_{max} of 2.7 in. (69 mm). As shown in Figure 4.3, resistance close to capacity for the five walls was sustained for a minimum of 0.5 in. (13 mm).

The parameter F_{yield} was used to compare the monotonic performance with the cyclic performance. F_{yield}, given in Table 4.1, ranged from 7.5 kips (33.4 kN) for Wall E (r = 0.30) to 35.6 kips (158 kN) for Wall A (r = 1.0). The ratio of F_{yield} to F_{max}, as given in Table 4.1, ranged from 0.86 to 0.92 for the five wall configurations. Due to the small range of the F_{yield} to F_{max} ratio, F_{yield} can reasonably be modeled as 89% of F_{max}.

Corresponding displacement, Δ_{yield}, given in Table 4.1, ranged from 0.48 in. (12 mm) to 0.98 in. (25 mm). Wall E (r = 0.30) was an outlier with a Δ_{yield} of 0.98 in. (25 mm). Drift at yield of the other four walls ranged from 0.48 in. (12 mm) to 0.57 in. (15 mm). As shown in Figure 3.1, the configuration of Wall E was unique. The other four walls had sheathing distributed throughout the length of the wall, while sheathing was only located at the extreme ends for Wall E. Figure 4.3 shows that the load-displacement curve of Wall E has lower magnitude loads and higher magnitude displacements than the other four configurations, resulting in the higher Δ_{yield}.

As given in Table 4.1, $F_{failure}$ ranged from 6.6 kips (29.4 kN) to 31.0 kips (137.9 kN). As previously stated, only Walls A and B experienced a sudden drop in load resistance. The sudden drop in resistance for both Walls A and B occurred very close to 80% of F_{max}. Drift corresponding to failure, $\Delta_{failure}$, given in Table 4.1, ranged from 4.00 in. (102 mm) for Wall C (r = 0.55) to 5.05 in. (128 mm) for Wall E (r = 0.30). For Walls A, B, and C, $\Delta_{failure}$ ranged from 4.00 in. (102 mm) to 4.18 in. (106 mm). For Walls D and E, which contained the largest openings, $\Delta_{failure}$ ranged from 5.04 in. (128 mm) to 5.05 in. (128 mm).

As sheathing and sheathing nailing increases, higher loads can be resisted. However, the sheathing nailing is at greater risk of being overstressed which will result in failure (usually in the form of pull through). This is the reason Walls A and B experienced sudden drops in load resistance. Conversely, nailing in walls with less sheathing, such as Walls D and E, are able to resist shear at increased drifts due to the added flexibility of the wall segments rocking at the base.

4.3.2 Elastic Stiffness

Elastic stiffness was determined at as the secant stiffness at 40% of capacity for the five wall configurations. The elastic stiffness values are given in Table 4.1 and illustrated as a function of sheathing area ratio in Figure 4.5. Elastic stiffness ranged from 7.8 kips/in (1370 kN/m) to 63.7 kips/in (11150 kN/m), with Wall E (r = 0.30) having the lowest stiffness and Wall A (r = 1.0) having the highest stiffness. This represents an 88% change in stiffness when the stiffness for the fully sheathed wall is used as the basis for comparison. A best fit regression determined the following second order equation for elastic stiffness as a function of sheathing area ratio:

$$k_e = 16.194 \cdot r + 48.847 \cdot r^2 \qquad (4.3)$$

where k_e is elastic stiffness and r is sheathing area ratio.

The area of sheathing, nailing schedule, location of openings, and anchorage are key factors effecting elastic stiffness. The number of full height panels adjacent to loading, and the path for shear force distribution around openings, effects the initial stiffness of the walls. Due to the large number of factors that effect elastic stiffness, a best fit

equation of elastic stiffness should encompass more variables than just sheathing area ratio.

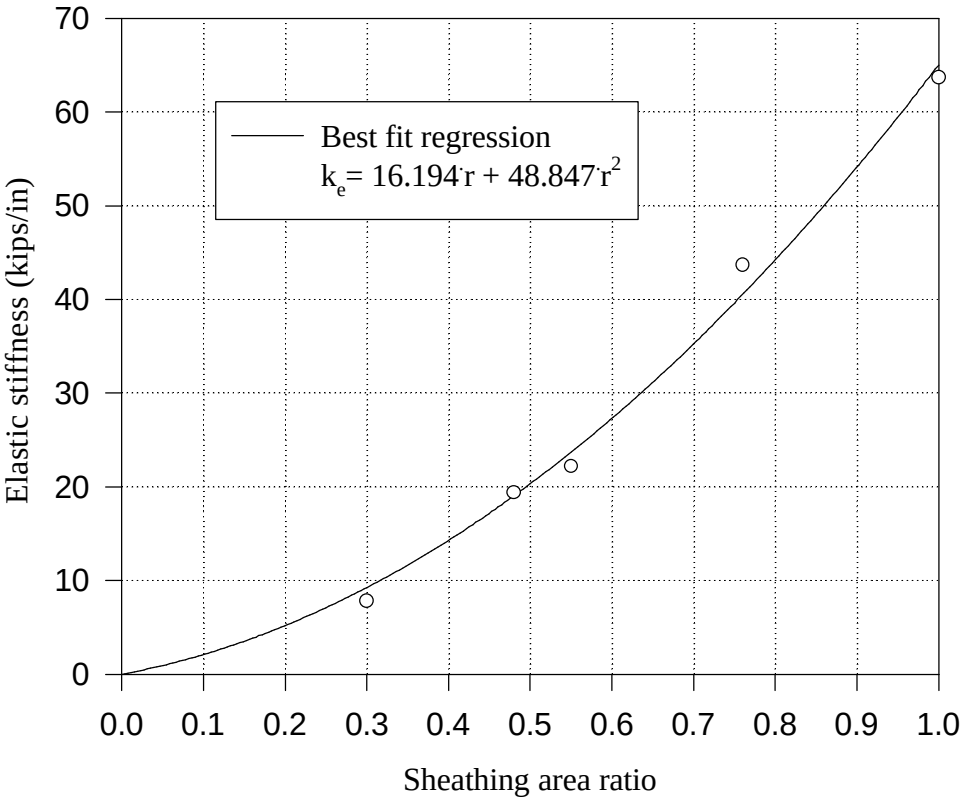

Figure 4. 5- Monotonic elastic stiffness of the five shear wall configurations examined plotted against sheathing area ratio

Figure 4.6 examines the relationship between capacity and elastic stiffness for the five shear wall configurations examined. Figure 4.6 plots the shear strength ratio on the x-axis versus shear stiffness ratio on the y-axis. Shear strength ratio was defined as the ratio of capacity of a shear wall divided by the capacity of the fully sheathed wall.

Similarly, shear stiffness ratio was defined as the ratio of elastic stiffness of a shear wall divided by the elastic stiffness of the fully sheathed shear wall. Although based on a limited number of tests, the data in Figure 4.6 tends to follow a one-to-one relationship between capacity and elastic stiffness.

4.3.3 Ductility

Ductility was determined using Equation 4.1. Table 4.1 shows that the ductility for the five wall configuration ranged between 5.2 and 8.8. Wall E had the lowest ductility ratio and was significantly lower than the other four wall specimens. The range of ductility for Walls A - D ranged from 7.3 to 8.8.

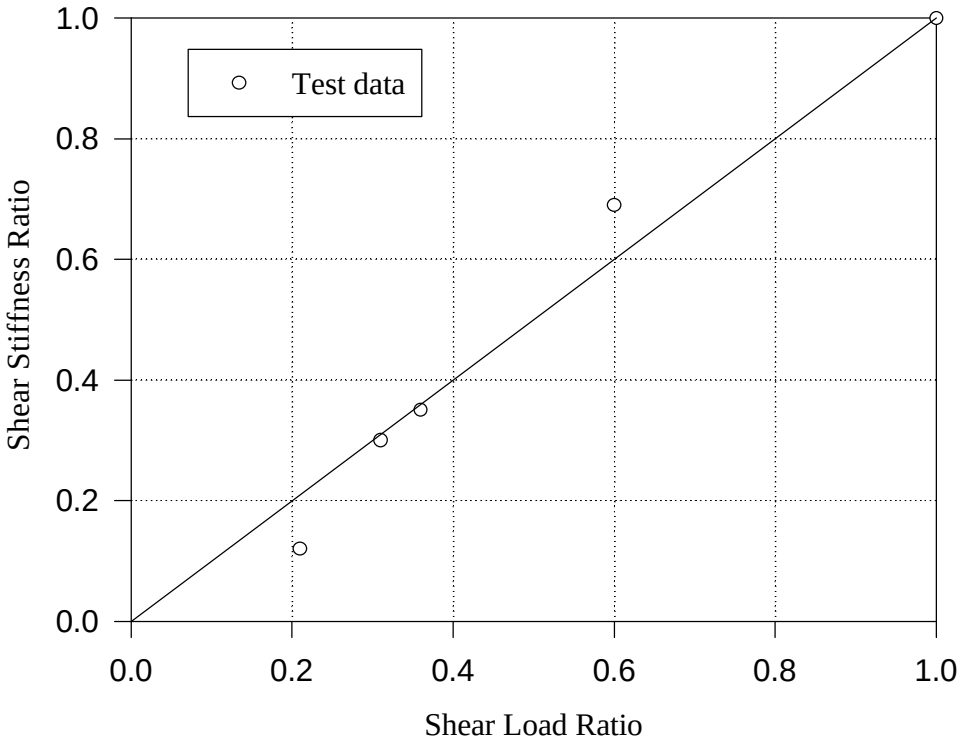

Figure 4. 6- Correlation of monotonic shear load ratio and stiffness ratio for the five shear wall configurations examined

Drift at failure, $\Delta_{failure}$, for Walls A (r = 1.0), Wall B (r = 0.76) and Wall C (r = 0.55) fell in the relatively small range of 4.00 in. (102 mm) to 4.18 in. (106 mm) and Δ_{yield} ranged between 0.48 in. (12 mm) and 0.56 in. (14 mm). However, due to the fact that Δ_{yield} is in the denominator of Equation 4.1, the ductility ratio is sensitive to small differences in Δ_{yield}. This results in Wall A (r = 1.0) having a ductility ratio of 7.4, Wall B (r = 0.76) having a ductility ratio of 8.7, and Wall C (r = 0.55) having a ductility ratio of 7.3. Even though these three walls had relatively similar load-displacement curves, ductility ranged form 7.3 to 8.7. This illustrates why the acceptable performance of structures can not be judged by considering ductility alone.

Walls D and E had similar load-displacement curves, both with $\Delta_{failure}$ over 5 in. (127 mm). However, due to the sheathing configuration Δ_{yield} of Wall E was much higher than the other four walls, resulting in a lower ductility. Δ_{yield} of Wall E was 72% higher than Δ_{yield} of Wall D. Wall D had a ductility ratio of 8.8 while Wall E had a ductility ratio of 5.2.

While providing an important indication of performance, ductility must be viewed in relation to stiffness, yield resistance, and capacity to provide an overall evaluation of monotonic performance.

4.3.4 Wall Behavior

Movement of the end studs relative to the foundation and performance of the tie-down anchors is discussed in this section. Due to computer error, the data pertaining to the end stud behavior and the slip of the tie-downs for Wall E (r = 0.30) wall was not recorded correctly. However, the other four walls provided quantitative information and the deflection pattern observed during the monotonic tests of Wall E was similar. Therefore, the behavior of the studs and anchor slip for this wall should be similar.

4.3.4.1 End Stud Movement

Loading each wall resulted in uplift zones and compression zones at the ends of the walls. On the uplift end of the wall, the end studs separated from the bottom plate. Separation was resisted by the sheathing nails and the tie-down anchor at the bottom of the studs. Uplift of the end studs was measured with LVDT #3, and Table 4.2 shows a relatively small magnitude of separation ranging between 0.08 in. (2 mm) to 0.18 in. (5 mm) at capacity. Without tie-down anchors connecting the end studs to the foundation, uplift measured would have been significantly higher. The effect of tie-down anchors on shear wall performance is currently being investigated and the results will be presented by Heine (1997).

On the compression end of the wall, the sheathing and compression strength perpendicular-to-grain of the sill plate resisted the overturning moment. It was observed prior to testing that each wall contained a small gap (less than 0.1 in. (2 mm)) between the end stud and the bottom sill plate. The displacement recorded with LVDT #2 recorded closure of this gap as well as crushing of the bottom sill plate. As shown in Table 4.2, movement of the end studs ranged from 0.06 in. (1.5 mm) to 0.126 in. (3 mm) at F_{max}. Only Wall A (r = 1.0) recorded movement greater than 0.09 in. (2 mm). Significant crushing of the bottom sill plate by the end studs was not observed.

4.3.4.2 Slip of Tie-Down Anchors

Shear wall failures in seismic events have resulted from slip or separation of the tie-down anchor from the end studs. For purposes of monitoring slip between anchor and end stud, a LVDT was placed on each metal tie-down anchor. After observing that slip of tie-down anchors relative to the double end studs for the majority of the tests was negligible, data regarding tension forces transmitted to the foundation by the tie-down anchor bolts was acquired for Wall C. For this reason, Wall C (r = 0.55), which was the last wall tested, does not have data regarding slip between tie-down anchors and end studs.

As shown in Table 4.2, the slip relative to the stud for anchors in tension, recorded near peak load, was less than 0.05 inches (1 mm), which is negligible. Figure 4.7 plots slip of the tension side tie-down against load resistance. Figure 4.8 plots drift against slip of the tension side tie-down anchors. A sudden drop in slip of the tension side tie-down anchor for both Walls A and B is recorded in Figures 4.7 and 4.8. In both cases,

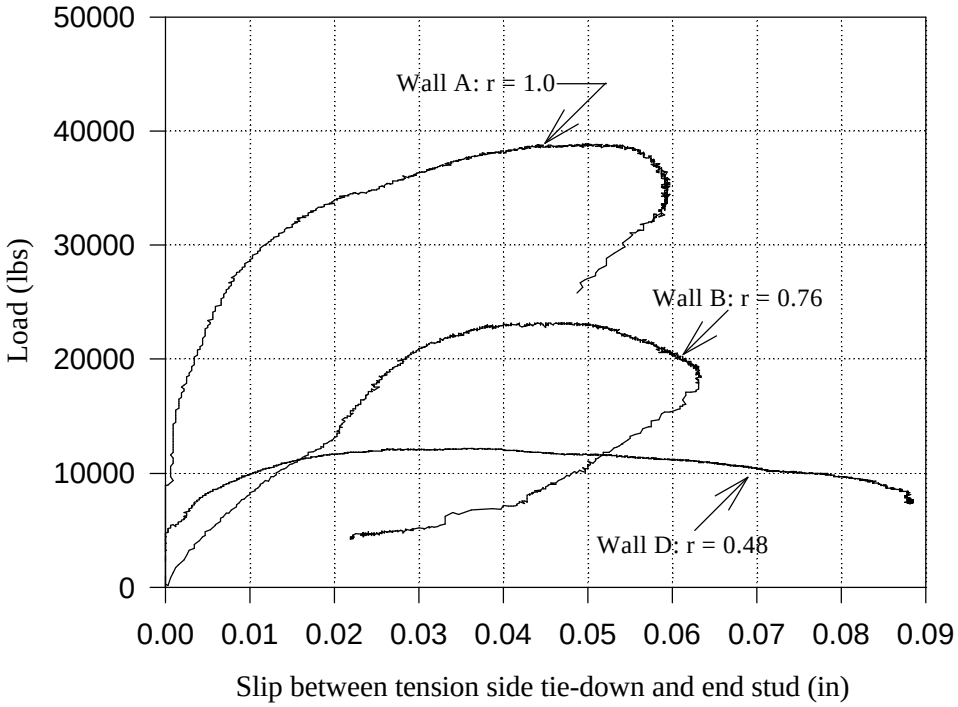

Figure 4. 7- Slip between tension side tie-down and end studs for Walls A, B and D plotted against lateral load resistance

Table 4. 2: Monotonic end stud displacement and tie-down slip at capacity for the five shear wall configurations examined

	Wall A	Wall B	Wall C	Wall D
	r = 1.0	r = 0.76	r = 0.55	r = 0.48
LVDT #3 - uplift of end studs	0.16 in. (4 mm)	0.08 in. (2 mm)	0.18 in. (5 mm)	0.09 in. (2 mm)
LVDT #2 - crushing of bottom plate	0.126 in. (3 mm)	0.06 in. (2 mm)	0.085 in. (2 mm)	0.086 in. (2 mm)
LVDT #5 - slip of tension side tie-down	0.048 in. (1 mm)	0.04 in. (1 mm)	*	0.024 in. (1 mm)
LVDT #6 - slip of compression side tie-down	0.0003 in. (0 mm)	0.008 in. (0 mm)	*	0.003 in. (0 mm)

* no data

the drop occurs after Δ_{max}, but before $\Delta_{failure}$ had been reached. This indicates that the first panel was unable to continue resist load prior to complete failure of the wall. After the first panel failed, the remaining panels had to resist the load until complete failure occurred.

Slip between the anchors and the end studs in compression never exceeded 0.003 in. (0.076 mm). Connection of the tie-down anchor to the double end studs with 32 16d sinker nails, as described in Section 3.3, did not experience significant slip and was therefore not a significant cause of failure.

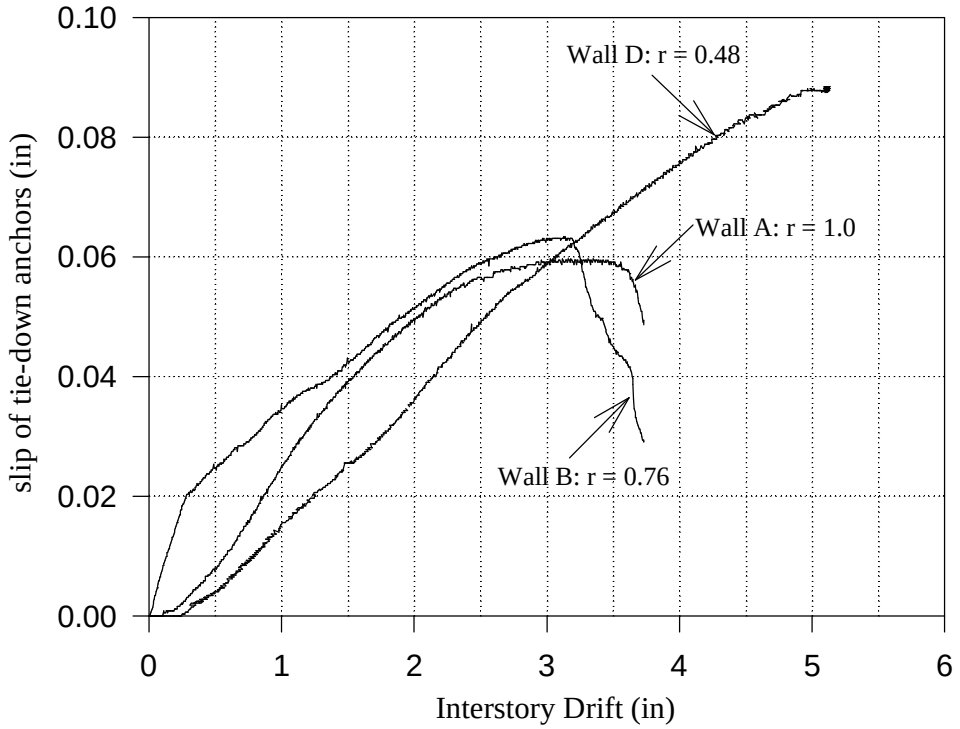

Figure 4. 8- Slip between tension side tie-down anchor and end studs for Walls A, B and D plotted against drift

4.3.4.3 Tension Bolts

Tension load bolts were used to connect the tie-down anchors to the foundation for the monotonic test of Wall C (r = 0.55). Figure 4.9 plots the load experienced by the tension side load bolt as a function of drift. For comparison, Figure 4.9 also includes the lateral load- drift curve for Wall C (r = 0.55). As shown in Figure 4.9, the tension anchor bolt initially resists more load than the wall. This is attributed to the reduced moment arm between the tension bolt and the center of rotation of the panel at low load magnitudes. Using conventional static methods, the sum of the moments in the first panel must balance. The moment resisted by the anchor bolt is equal to the magnitude of the force resisted mulitplied by the moment arm (the distance from the

anchor bolt to the center of rotation of the panel). The exterior edges of the plywood end panels are attached with two rows of 8d sheathing nails, which results in the panel rotating closer to the double row of nailing rather than the center of the panel. As the double row of sheathing nails sustain higher stresses and becomes more flexible, the center of rotation moves closer to the center of the panel. For this reason, the moment arm is reduced at low load magnitudes and results in higher forces in the anchor bolt than the lateral load resisted by the shear wall.

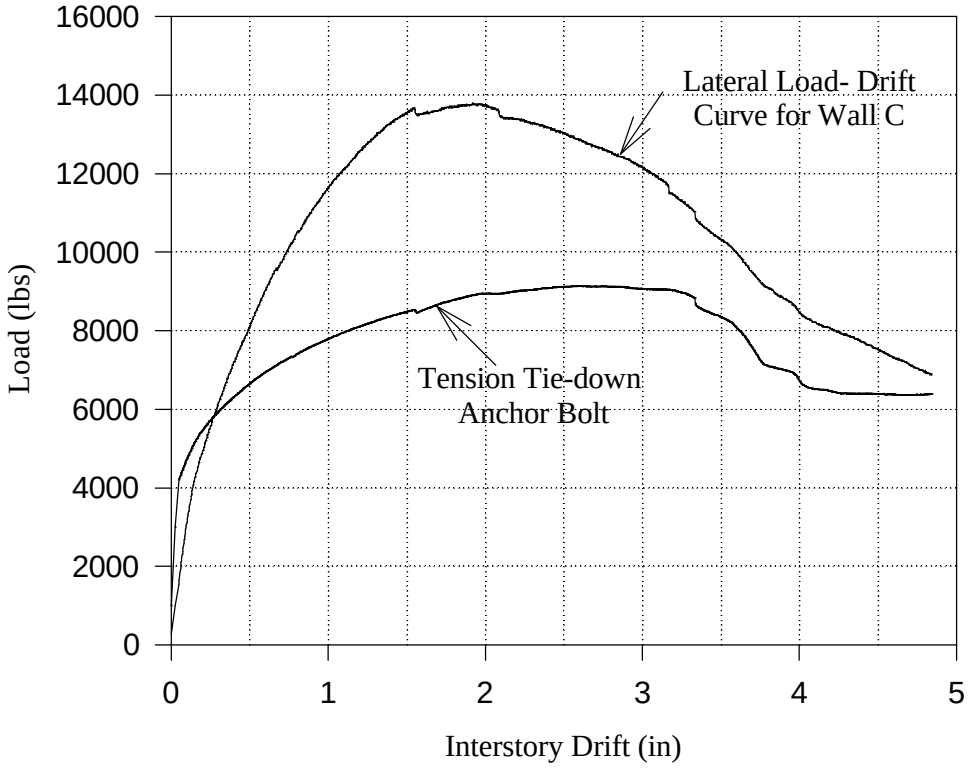

Figure 4. 9- Tension side tie-down anchor bolt load resistance of Wall C plotted against drift

Shear distribution is not uniform in walls with openings because full height panels at the ends of the walls resist more shear than other full height panels due to the tie-down anchorage. The best estimate of panel shear capacity for panels adjacent to the tension side tie-down are based on results from the fully sheathed wall. From the test of Wall A (r = 1.0), the unit shear capacity equals 38,800 lbs / 40 ft or 970 plf. The overturning couple design value would then be determined as 970 plf (14.2 kN/m) times the wall height of 8 ft (2.4 m), or 7760 lbs (34.5 kN). The actual peak load experienced by the tension side anchor bolt was 8900 lbs (39.6 kN), which exceeds the expected value by 15%. This performance parameter should be investigated in more detail in future experimental tests.

4.3.4.4 Modes of Failure

All of the walls tested under monotonic loading had similar failure characteristics. Typically, each wall performed relatively elastically until a drift of about 0.50 in. (13 mm) at which point the stiffness of the walls began to decrease. There was no apparent visual damage to the walls at this point.

At a drift near 1 in. (25.4 mm), the walls underwent some minor damage but load resistance was still increasing. All drywall tape joints around openings cracked, and some tape joints between full drywall panels had failed at this drift. Drywall nails near the corners of panels had begun to fail, while field nailing of gypsum board still performed adequately. Racking of plywood panels was observed for fully sheathed panels, while the plywood above and below windows acted as a rigid body.

As load capacity of the walls plateaued, bending of the plywood sheathing near the loaded end was observed in some instances. Bending of plywood nails caused crushing of the plywood around the nail hole, decreasing friction between wooden elements and sheathing nailing. After peak capacity had been reached, the nails usually tore through in the edges of plywood. Nails in the buckled panels showed both nail pull out from the framing (top and bottom plates) and nail head pull through. As this failure mode progressed, the nails progressively failed along the bottom plate in the walls with openings. This progressive failure along the bottom plate (unzipping) occurred in the wall sections that had no tie-down anchor to resist the uplift on the tension side. These failures usually showed signs of the nails tearing out of the plywood edge or pulling through the plywood leaving a small hole. At large deformations the edge nails tore through the edge of the gypsum or the head pulled through the gypsum panel.

4.4 Prediction of Capacity

This section presents two methods for capacity prediction of shear walls with openings that only have tie-down anchorage at the ends of the wall. Both prediction methods rely upon the known capacity of the fully sheathed wall with identical materials and dimension. Because actual capacity of the fully sheathed wall is usually not known in design situations, the ultimate capacity determined from current design procedures used in the 1994 UBC can be used in the two prediction methods. For this reason, this section first discusses the capacity using current design procedures and then examines the two prediction methods.

4.4.1 Current Design Capacity

Current design procedures only include full height wall panels to distribute shear. To determine the capacity of a shear wall, the following equation is used:

$$V_{wall} = (V_{ply,\,ult} + V_{gyp,\,ult}) \cdot \text{Length of full height sheathing} \qquad (4.4)$$

where V_{wall} is the ultimate capacity of the shear wall, $V_{ply,ult}$ is the ultimate shear for plywood sheathing and $V_{gpy,ult}$ is the ultimate shear for the gypsum wallboard.

From Table 23-I-K-1 of the 1994 Uniform Building Code (UBC), the allowable shear for 15/32 in. (12 mm) structural I plywood with 8d nails at 6 in. (152 mm) perimeter spacing is 280 plf (4100 N/m). This design value assumes proper anchorage is provided at the ends of all full height wall segments to resist uplift. A factor of 0.82 must be applied to this value to account for the lower specific gravity of the spruce-pine-fir framing used in this experimental study. From APA PRP-108, shear wall criteria is based on a minimum load factor of 2.8.

According to Chapter 25 of the 1994 UBC, the allowable shear for gypsum board is 100 plf (1500 N/m). A minimum load factor of 2.5 is taken for the gypsum.

Using the allowable shears and load factors just described, the ultimate design shear of full height wall segments is determined as:

$$V_{wall} = \left[280 \text{ plf} \cdot (2.8) \cdot (0.82) + 100 \text{ plf} \cdot (2.5)\right] \cdot 40'$$
$$= 35{,}700 \text{ lbs } (158.8 \text{ kN})$$

This capacity compares well with the actual capacity for Wall A (r = 1.0) of 38,800 lbs (172.6 kN), and corresponds to a unit shear of 890 plf (13000 N/m).

The walls examined in this thesis only contained tie-down anchorage at the ends of the wall, thus making Wall A, the fully sheathed wall, the only wall with adequate anchorage provided. Walls that contained openings contained two shear wall panels with only one tie-down anchor (only one of the tie-downs was in tension) and the other shear wall panels (if any) did not contain tie-down anchors at all. Wall B (r = 0.76) consisted of three wall panels, Walls C and D consisted of four wall panels and Wall E consisted of two. It is noted that shear is not uniformly distributed in walls with openings. End panels resist greater shear relative to interior full height panels due to the double row of end nailing and the tie-down anchors. To demonstrate that allowable shears given in Table 23-I-K-1 of the 1994 UBC are not applicable to shear wall panels without proper tie-down anchorage, the unit shear of 890 plf (13000 N/m) is applied to the five wall configurations in Table 4.3. As shown, only the design value of the fully sheathed wall is lower than the actual capacity, indicating that tie-down anchorage at the ends of the wall only is not sufficient to achieve full engineered capacity for shear walls with openings. Capacity per length of full height sheathing panels ranged from 680 plf (9900 N/m) to 860 plf (1260 N/m) for Walls B - E.

4.4.2 Sugiyama's Empirical Prediction Equations

The results from three independent studies of one-third scale monotonic racking tests of typical North American, plywood-sheathed shear walls with openings are presented in Yasumura and Sugiyama (1984). Load required to displace the top of the wall at

apparent shear deformation angles of 1/60, 1/75, 1/100, 1/150, and 1/300 was collected for each test. Apparent shear deformation angle, γ, was defined as displacement of the top of wall, δ_{top}, minus displacement of the bottom of wall, δ_{bottom}, divided by total height, h, and is shown in Equation 4.5:

$$\gamma = \frac{\delta_{top} - \delta_{bottom}}{h} \tag{4.5}$$

Sugiyama et al (1994) presents an empirical equation for the calculation of the shear load ratio, f, of a shear wall segment with openings for an apparent shear deformation angle of 1/100 radian. Shear load ratio is defined as the ratio of the strength of a wall with openings to the strength of the fully sheathed wall. Shear load ratio, f, at an apparent shear deformation angle of 1/100 was calculated by the following expression:

$$f = \frac{r}{3 - 2 \cdot r} \tag{4.6}$$

where r is sheathing area ratio (Equation 3.1). It had been proposed that Equation 4.6 is applicable for prediction of capacity for typical light-frame shear walls.

Sugiyama et al (1994) determined additional empirical equations (referred to as the W.U. equations) relating load and sheathing area ratio, based on all the tests performed for apparent shear deformation angles of 1/60, 1/100 and 1/300. These equations determine the shear load ratio at a particular apparent shear deformation angles. For a shear deformation angle of 1/60 radians:

$$f = \frac{r}{2 - r} \tag{4.7}$$

For a shear deformation angle of 1/300 radians:

$$f = \frac{3 \cdot r}{8 - 5 \cdot r} \tag{4.8}$$

where f is shear load ratio and r is sheathing area ratio.

For an 8 ft. (2.4 m) high wall, shear deformation angles of 1/300, 1/100, and 1/60 correspond to racking displacements of 0.32 in. (8 mm), 0.96 in. (24 mm), and 1.6 in. (41 mm), respectively.

Predicted capacity of shear walls with openings is obtained by multiplying the shear load ratio, f, by the actual capacity of the fully sheathed wall. However, the actual capacity is not known in design situations. For this reason, predictions determined from Equation 4.6, using the capacity of the fully sheathed wall determined in Section 4.4.1 as the reference capacity are also presented.

Table 4. 3: Comparison of monotonic capacity of the five shear wall configurations examined with ultimate design capacity

	Wall A r = 1.0	Wall B r = 0.76	Wall C r = 0.55	Wall D r = 0.48	Wall E r = 0.30
Actual Capacity (kips)	38.8/0.97	23.1/0.83	13.8/0.86	12.1/0.76	8.2/0.68
Design Capacity (kips)	35.7/0.89	25.0/0.89	14.3/0.89	14.3/0.89	10.7/0.89
Actual / Design	1.11	0.92	0.97	0.85	0.77

Table 4.4 compares actual load resistance at 0.32 in. (8 mm), 0.96 in. (24 mm), 1.6 in. (41 mm) and capacity with the predicted load resistance. Also included in Table 4.4 are the actual and predicted shear load ratios, where shear load ratio is as previously defined. The ratio of actual load resistance to predicted load resistance is included in Table 4.4, where a ratio greater than 100% indicates a conservative prediction by Sugiyama's empirical equations and a ratio less than 100% indicates an unconservative prediction by Sugiyama's empirical equations.

Capacity predictions made by Equation 4.6 are compared in Table 4.4 and Figure 4.9 using both the actual experimental capacity of Wall A and the design capacity determined in Section 4.4.1 as the reference capacity. The use of the actual experimental capacity of the fully sheathed wall condition as the reference capacity is used to verify Sugiyama's empirical method. Predictions based on the design capacity are only provided to show the applicability in design. With the actual capacity of the fully sheathed wall used as the reference, Table 4.4 shows that the actual to predicted ratio is 100% to 168%. When the design capacity is used as the reference, the actual to predicted ratio ranged from 111% to 178%. In both cases, Equation 4.6 makes conservative predictions. It is noted that as the sheathing area ratio decreases (i.e. amount of openings increase), the more conservative capacity predictions become. Figure A-1 in Appendix A plots capacity data from this thesis and Rose and Keith (1995). As shown in Figure A-1, predictions made using Equation 4.6 were conservative in all cases.

At a drift of 0.32 in. (8 mm), Equation 4.8 is used to predict shear load ratios. Table 4.4 shows that the actual to predicted ratio is 98% to 117%. Sugiyama's equation was slightly unconservative for Wall E (r = 0.30) at this drift. However, predictions made by Equation 4.8 at 0.32 in. (8 mm) are more representative of the actual load resistances determined in this investigation relative to predictions made at capacity. This is advantageous for analyzing existing structures.

Table 4. 4: Comparison of actual load resistances at capacity and drifts of 0.32 in., 0.96 in., and 1.6 in. for the five shear wall configurations examined with load resistance's determined from Sugiyama's shear load ratio equations

	Wall A	Wall B	Wall C	Wall D	Wall E
	r = 1.0	r = 0.76	r = 0.55	r = 0.48	r = 0.30
Peak Load (kips)	38.8	23.1	13.8	12.1	8.2
Actual Shear Load Ratio	1.0	0.60	0.36	0.31	0.21
Predicted Shear Load Ratio	1.0	0.51	0.29	0.24	0.13
Eqn 4.6 Predicted Capacity (kips) with Actual Capacity as reference	38.8	19.9	11.2	9.1	4.9
Actual Capacity / Predicted Capacity	100%	117%	122%	132%	168%
Eqn 4.6 Predicted Capacity (kips) with Design Capacity as reference	35.7	18.2	10.4	8.6	4.6
Actual Capacity / Predicted Capacity	109%	127%	133%	141%	178%
@0.32 in. drift (γ = 1/300)					
Actual Load (kips)	18.5	11.4	6.3	5.5	2.5
Predicted Load (kips) (Eqn 4.8)	18.5	10.0	5.8	4.8	2.6
Actual Shear Load Ratio	1.0	0.62	0.34	0.30	0.14
Predicted Shear Load Ratio	1.0	0.54	0.31	0.26	0.14
Actual Load / Predicted Load	100%	114%	109%	117%	98%
@0.96 in. drift (γ = 1/100):					
Actual Load (kips)	33.6	20.0	11.4	11.0	6.3
Predicted Load (kips) (Eqn 4.6)	33.6	17.3	9.7	7.9	4.2
Actual Shear Load Ratio	1.0	0.60	0.34	0.33	0.19
Predicted Shear Load Ratio	1.0	0.51	0.29	0.24	0.13
Actual Load / Predicted Load	100%	116%	117%	140%	152%
@1.6 in. drift (γ = 1/60):					
Actual Load (kips)	37.7	22.6	13.5	12.1	7.4
Predicted Load (kips) (Eqn 4.7)	37.7	23.1	14.3	11.9	6.6
Actual Shear Load Ratio	1.0	0.60	0.36	0.32	0.20
Predicted Shear Load Ratio	1.0	0.61	0.38	0.32	0.18
Actual Load / Predicted Load	100%	98%	94%	102%	111%

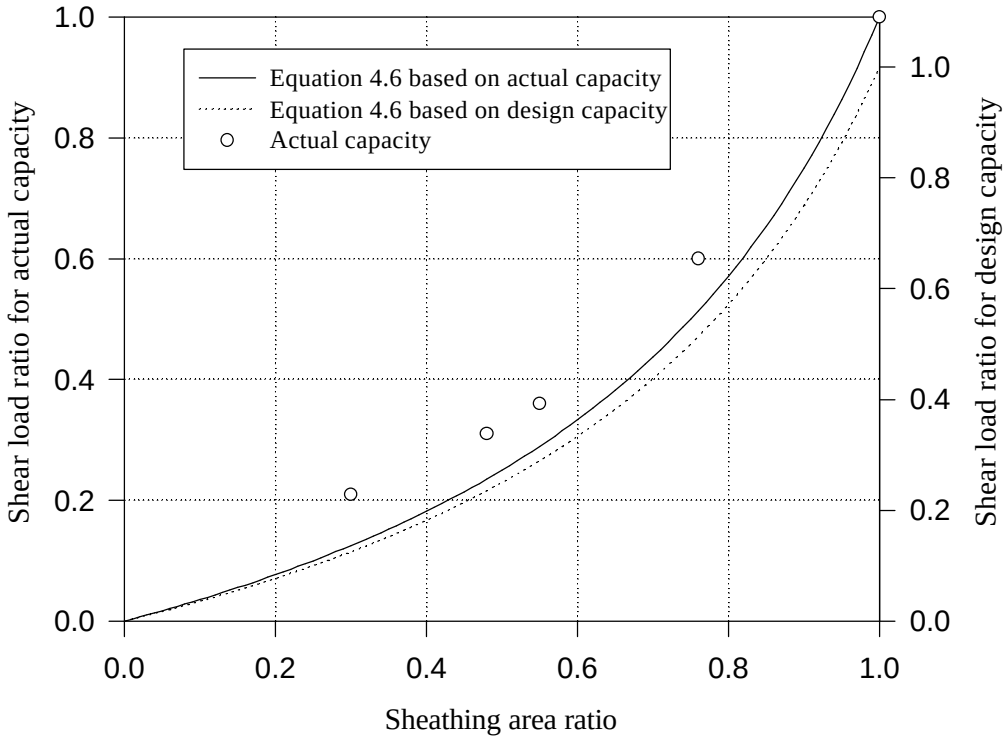

Figure 4. 10- Actual monotonic shear load ratios at capacity of the five shear wall configurations examined and Sugiyama's shear load ratio prediction equation plotted against sheathing area ratio

At a drift of 0.96 in. (24 mm), Equation 4.6 was used to predict shear load ratios. Table 4.4 shows that the actual to predicted ratio is 100% to 152%. Similar to Sugiyama's equations at capacity, as the sheathing area ratio decreases, the more conservative Equation 4.6 becomes. Figure A-2 in Appendix A plots data determined at an apparent shear deformation angle of 1/100 with data ,determined from Wakatsuki and Uchida (referenced in Sugiyama and Matsumoto, 1994.) Equation 4.6 is conservative for the majority of the one-third scale tests performed by Wakatsuki and Uchida.

At a drift of 1.6 in. (41 mm), Equation 4.7 is used to predict shear load ratios. Table 4.3 shows that the actual to predicted ratio is 94% to 111%. Predictions at 1.6 in. (41 mm) based on Equation 4.7 were slightly unconservative for Wall C (r = 0.55) and Wall B (r = 0.76). The predictions determined at 1.6 in. (41 mm) drift are a closer representation of the actual data, but is slightly less conservative than predictions at 0.32 in. (8 mm). It is also noted that all of the wall configurations tested reached capacity at or above 1.6 in. (41 mm) drift.

A method of predicting elastic stiffness would be beneficial for design and analysis. The use of Sugiyama's empirical equations have been applied to stiffness prediction at a drift of 0.32 in. (8 mm). At this drift, Figure 4.3 shows that the five wall

configurations were behaving elastically. The predicted load resistance at 0.32 in. (8 mm) drift, determined using Equation 4.8, is divided by 0.32 in. (8 mm) to determine to predicted stiffness. Equation 4.6 was also used to predict load resistance at 0.32 in. (8 mm) and elastic stiffness. The predicted elastic stiffness' are compared in Table 4.5. Using Equation 4.6, predicted elastic stiffness ranged from 7.5 kips/in (1300 kN/m) to 57.8 kips/in (10100 kN/m), and was 4% to 49% higher than actual elastic stiffness.

Table 4. 5: Comparison of monotonic elastic stiffness of the five shear wall configurations examined with elastic stiffness determined from Sugiyama's shear load ratio equations

	Wall A r = 1.0	Wall B r = 0.76	Wall C r = 0.55	Wall D r = 0.48	Wall E r = 0.30
Actual Elastic Stiffness (kips/in)	63.7	43.7	22.2	19.4	7.8
Actual Stiffness Ratio	1.0	0.69	0.35	0.30	0.12
Actual Load Resistance @ 0.32 in.	18.5	11.4	6.3	5.5	2.5
Actual Load Ratio @ 0.32 in.	1.0	0.62	0.34	0.30	0.14
Load Resistance Predicted @ 0.32 in. (kips) (Eqn 4.6)	18.5	9.4	5.4	4.4	2.4
Predicted Stiffness (kips/in) (=predicted load/ 0.32 in.)	57.8	29.4	16.9	13.8	7.5
Actual Stiffness / Predicted Stiffness	1.10	1.49	1.31	1.41	1.04
Load Resistance Predicted @ 0.32 in. (kips/in) (Eqn 4.8)	18.5	10.0	5.8	4.8	2.6
Predicted Stiffness (kips/in) (=predicted load/ 0.32 in.)	57.8	31.3	18.1	15.0	8.1
Actual / Predicted Stiffness	1.10	1.40	1.23	1.29	0.96

Using Equation 4.8, predicted elastic stiffness ranged from 8.1 kips/in (1400 kN/m) to 57.8 kips/in (10100 kN/m). The predicted elastic stiffness of Walls A - D were 10% to 40% higher than actual. Predicted stiffness of Wall E was 4% lower than actual. When compared to actual elastic stiffness, Equation 4.8 predicts closer than Equation 4.6. However, both over predict stiffness.

When predicted stiffness is used to calculate estimated drifts, unconservative estimates of drifts are found (i.e. estimated drifts are lower than actual). When predicted

stiffness is used to calculate estimated load, unconservative load estimates are found (i.e. estimated load is higher than actual).

4.4.3 Natural Log Prediction Method

Although Sugiyama's predictions were found to be conservative at capacity for all wall specimens tested, the prediction equations became overly conservative as the amount of openings increased. It is desirable to find a better prediction equation that has better precision (i.e. similar reserve capacities) at all sheathing area ratios.

The method of prediction presented here for shear walls with openings and tie-down anchorage at the extreme ends of the wall is referred to as the natural log method. It is based on capacity data from the five shear walls examined. The natural log of the capacities of the five shear walls were plotted against sheathing area ratio, and a linear regression was found to fit the data well. Keeping the slope constant, the natural log method adjusts the y-intercept of the best fit linear regression so that the equation predicts the capacity of the fully sheathed wall condition determined from current design methodology with conservative load factors. The same procedure is also done for prediction of cyclic capacity in Section 5.6.3. As shown in Figure 4.11, the natural log of F_{max} and the natural log of the actual shear load ratio was plotted against sheathing area ratio and a first order regression fits the data very well. The equation of the regression is as follows:

$$LN(F_{max}) = 1.420 + 2.24 \cdot r \qquad (4.9)$$

where F_{max} is capacity, and r is sheathing area ratio.

To determine the natural log method prediction equation, the y-intercept of Equation 4.9 is lowered so that the design capacity of the fully sheathed wall condition is predicted. The natural log method prediction equation for monotonic capacity is:

$$LN(F_{max}) = 1.335 + 2.24 \cdot r \qquad (4.10a)$$

where F_{max} is capacity and r is sheathing area ratio.

The corresponding natural log method prediction equation for predicted shear load ratios is:

$$LN(f) = -2.24 + 2.24 \cdot r \qquad (4.10b)$$

where f is the shear load ratio and r is sheathing area ratio. To determine capacity, F_{max}, multiply the shear load ratio, f, by the capacity determined through current design methodology with conservative load factors.

Table 4.6 tabulates the actual capacity of each wall with capacity determined from Equation 4.10a. The ratio of actual capacity to capacity from the best fit regression of the natural log of capacity fell in the range of 106% to 111%. For sheathing area

ratios between 0.3 and 1.0, the natural log method gave conservative predictions of capacity.

Unlike Sugiyama's predictions, similar reserve capacity is determined for the five wall configurations. Figure A-3 in the appenidix plots the natural log prediction equation with data from this investigation and from Rose and Keith (1995). The natural log method gave conservative predictions from Rose and Keith's (1995) data.

Equations 4.10a and 4.10b can be solved for capacity, F_{max}, and predicted shear load ratios, f,:

$$F_{max} = e^{(1.335+2.24 \cdot r)} \quad (4.10c)$$

$$f = e^{(-2.24+2.24 \cdot r)} \quad (4.10d)$$

Then if a safety of factor of 3.0 is desired, the design value would be

$$F_{design} = \frac{F_{max}}{3.0} = \frac{e^{(1.335+2.24 \cdot r)}}{3.0} \quad (4.8e)$$

$$f_{design} = \frac{f}{3.0} = \frac{e^{(-2.24+2.24 \cdot r)}}{3.0} \quad (4.8f)$$

where F_{design} is the allowable shear capacity of the wall and f_{design} is the allowable shear load ratio.

Equations 4.10e and 4.10f can be used to predict the actual wall racking capacity and ensure a reasonably uniform factor of safety.

Table 4. 6: Comparison of monotonic capacity of the five shear wall configurations examined with capacity determined from natural log method

	Wall A	Wall B	Wall C	Wall D	Wall E
	r = 1.0	r = 0.76	r = 0.55	r = 0.48	r = 0.30
Actual F_{max}	38.8	23.1	13.8	12.1	8.2
Predicted F_{max}	35.7	20.9	13.0	11.1	7.4
Actual/ Pred.	109%	111%	106%	109%	111%

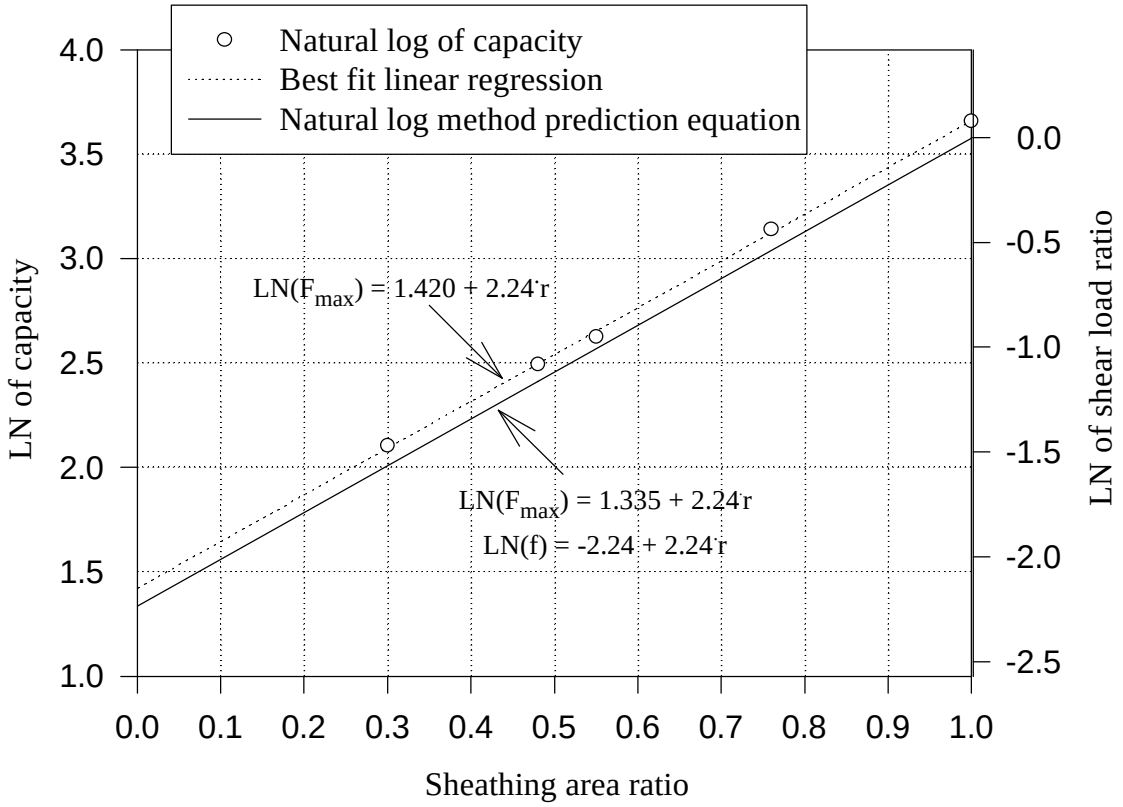

Figure 4. 11- Natural log of monotonic capacity of the five shear wall configurations examined and the natural log method prediction equation plotted against sheathing area ratio

The applicability of prediction, based on the natural log of capacity, developed in this research is limited due to the small number of variables examined. However, a linear empirical equation predicting the natural log of capacity based on framing, sheathing, sheathing nailing, tie-down anchorage, openings and wall length potentially can be determined with more shear wall tests examining more variables found in typical shear wall construction. For example, a possible prediction equation encompassing sheathing area ratio and nailing schedule would be of the form:

$$F_{design} = \frac{e^{(y_1 + y_2 \cdot r + y_3 \cdot n)}}{3.0}$$

where F_{design} is allowable design capacity, r is sheathing area ratio, n is a nailing schedule factor, and y_1, y_2, and y_3 are regression coefficients.

The same methodology used to determine capacity prediction with the natural log method is applied to predict elastic stiffness. There is one drawback to stiffness prediction, and that is there is not a design elastic stiffness to use as a reference. Figure 4.12 is similar to Figure 4.11, but the natural log of elastic stiffness is plotted instead of capacity. The best fit regression fits best when Wall E was excluded, so a

higher lower limit on sheathing area ratio may be necessary for elastic stiffness estimates. The natural log best fit equation for elastic stiffness is:

$$LN(k_e) = 1.85 + 2.36 \cdot r \qquad (4.11)$$

where k_e is elastic stiffness and r is sheathing area ratio.

From Table 4.7, the actual to predicted ratio ranged from 95% to 114%. These are good estimates of elastic stiffness, but more data needs to be applied to the natural log method to determine its validity for a larger range of shear walls.

Although beyond the scope of this thesis, existing monotonic data with openings should be examined to determine if the natural log method can be used to design shearwalls with openings with better accuracy.

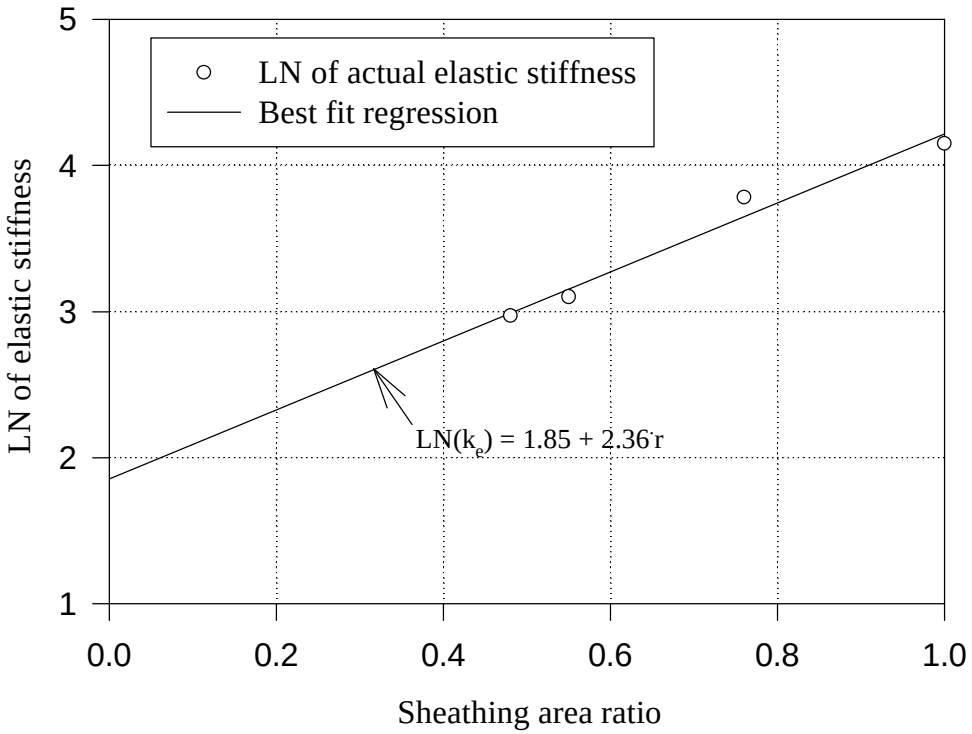

Figure 4. 12- Natural log of monotonic elastic stiffness of the five shear wall configurations examined, and the natural log method prediction equation plotted against sheathing area ratio

4.5 Conclusions

The data from the monotonic shear wall tests has been presented and the following conclusions were drawn:

- Sheathing above and below openings resists shear

- Slip of nailed tie-down anchorage, relative to the end studs, did not occur
- Gypsum sheathing helps resist shear in the low to moderate loading, but the plywood sheathing is the predominant shear resisting element near capacity
- Pull through of the plywood sheathing nails was the predominant mode of failure
- Current estimation of tie-doen forces was shown to be unconservative for one wall. Further research is needed to investigate this concern.
- Sugiyama's method of prediction of shear walls with openings at capacity was found to be conservative for the five wall configurations examined
- The natural log prediction method, although based on a limited data, provides good prediction of capacity and stiffness of shear walls in this study

Table 4. 7: Comparison of monotonic elastic stiffness of the five shear wall configurations examined with elastic stiffness determined from the natural log method

	Wall A r = 1.0	Wall B r = 0.76	Wall C r = 0.55	Wall D r = 0.48
Actual elastic stiffness (kips/in)	63.7	43.7	22.2	19.4
Natural log elastic stiffness (kips/in)	67.4	38.2	23.3	19.7
Actual / predicted	95%	114%	95%	98%

4.6 Summary

This chapter has dealt with the data from the monotonic shear wall tests. Load - drift and equivalent elastic-plastic curves were determined for each wall configuration. Capacity, elastic stiffness and ductility results were discussed. Performance of the tie-down anchors was evaluated. Slip between tie-downs and the end studs was determined not to be a cause of failure. Movement of the end studs, relative to the bottom plate, was measured. This movement was significantly reduced by the tie-down anchors. Pure tension load bolts were used to connect the foundation to the tie-down anchors for one monotonic wall configuration. Two methods of prediction were discussed and shown to give conservative results.